Characterization by Raman Microspectroscopy of the Strain-Induced Conformational Transition in Fibroin Fibers from the Silkworm *Samia cynthia ricini*

Marie-Eve Rousseau,[†] Lilyane Beaulieu,[†,‡] Thierry Lefèvre,[†] Joanie Paradis,[†] Tetsuo Asakura,[‡] and Michel Pézolet*[,†]

Département de Chimie et CERSIM, Université Laval, Québec, QC, Canada G1K 7P4, and Department of Biotechnology, Tokyo University of Agriculture and Technology, Japan

Received March 22, 2006; Revised Manuscript Received May 19, 2006

Raman microspectroscopy has been used to quantitatively study the effect of a mechanical deformation on the conformation and orientation of *Samia cynthia ricini* (*S. c. ricini*) silk fibroin. Samples were obtained from the aqueous solution stored in the silk gland and stretched at draw ratios (λ) ranging from 0 to 11. Using an appropriate band decomposition procedure, polarized and orientation-insensitive spectra have been analyzed to determine order parameters and the content of secondary structures, respectively. The data unambiguously show that, in response to mechanical deformation, *S. c. ricini* fibroin undergoes a cooperative α-helix to β-sheet conformational transition above a critical draw ratio of 4. The α-helix content decreases from 33 to 13% when λ increases from 0 to 11, while the amount of β-sheets increases from 15 to 37%. In comparison, cocoon silk is devoid of α-helical structure and always contains a larger amount of β-sheets. Although the presence of isosbestic points in different spectral regions reveals that the conformational change induced by mechanical deformation is a two-state process, our results suggest that part of the glycine residues might be incorporated into β-poly(alanine) structures. The β-sheets are initially isotropically distributed and orient along the fiber axis as λ increases, but do not reach the high level of orientation found in the cocoon fiber. The increase in the orientation level of the β-sheets is found to be concomitant with the $\alpha \rightarrow \beta$ conformational conversion, whereas α-helices do not orient under the applied strain but are rather readily converted into β-sheets. The components assigned to turns exhibit a small orientation perpendicular to the fiber axis in stretched samples, showing that, overall, the polypeptide chains are aligned along the stretching direction. Our results suggest that, in nature, factors other than stretching contribute to the optimization of the amount of β-sheets and the high degree of orientation found in natural cocoon silk.

Introduction

Fibers rank among the stiffest and strongest materials manufactured by man or found in nature. Biological fibrous materials are currently under intense investigation to learn how to improve and produce novel fibers and other high-performance materials.[1−3] In recent years, the tensile properties of spider and lepidopteran silks have aroused considerable interest. The production of biopolymers derived from silk is an attractive way to capitalize on silk's high strength, stiffness, and extensibility.[3,4] By means of biotechnologies, there has been considerable progress toward the production of recombinant spider silk proteins of high molecular weight.[5−10] Since the mass-production of recombinant silk proteins is now feasible, the greatest challenge is to produce usable biomaterials with desired mechanical properties. The achievement of this goal depends on the processability of such proteins and our ability to mimic nature's perfection to self-assemble them into a thread.[11−14]

The remarkable mechanical properties of natural silk are intimately related to its structural organization. Indeed, the conformation of proteins and their orientation in silk filaments are judiciously adapted to create a highly structural material. Precise control of the proteins' hierarchical molecular order is maintained by the primary amino acid sequence combined with processing conditions during spinning. Since similar control is desirable when processing silk-based biopolymers, it is of crucial interest to fully understand the spinning process by which the bulk silk secretions are converted into an insoluble thread. In nature, the spinning occurs in an aqueous medium whose environment (pH, concentrations of ions) changes along the spinning duct.[15−18] It has also been suggested that the formation of a liquid crystalline state along the duct plays a pivotal role in protein self-assembly and microstructure.[19−21] However, other important physical factors, such as elongation flow, shear stress, dehydration, and mechanical drawing, also need to be considered. The importance of each of these parameters on the final silk structure still remains unclear, and they will have to be studied to maximize our effectiveness in copying the natural spinning process.

Molecular orientation in fibrous materials is known to favorably influence the tenacity of the fibers. For example, the impact of a mechanical deformation on the tensile properties of regenerated silk fibers has already been noted,[8,19,22−27] but its effects on the conformation and orientation of the silk proteins at the molecular level is far from being elucidated. Therefore, further investigation of natural spinning systems, and especially the effect of a mechanical drawing, is needed. In this respect, the wild silkworm *Samia cynthia ricini* (*S. c. ricini*) is an interesting species to study since the protein primary structure of the silk it produces is quite similar to that of spider dragline

* To whom correspondence should be addressed. Phone: (418) 656-2481. Fax: (418) 656-7916. E-mail: michel.pezolet@chm.ulaval.ca.
[†] Université Laval.
[‡] Tokyo University of Agriculture and Technology.

10.1021/bm060280w CCC: $33.50
Published on Web 08/19/2006

silk. Indeed, both types of silk contain alanine repetitive sequences interleaved with glycine-rich domains, although the alanine motif is longer in *S. c. ricini* cocoon silk[28] (10−13 residues) compared to that of *Nephila clavipes* (*N. clavipes*) dragline silk (5−7 residues).[29,30] Although their amino acid sequence is not exactly the same, it has recently been shown that *S. c. ricini* cocoon silk and *N. edulis* spider dragline give similar polarized Raman spectra,[31] thus suggesting similar secondary structures.

Several studies have shown that β-sheet is the dominant conformation in cocoon silk spun by *S. c. ricini*.[31−33] However, the α-helix seems to be the dominant ordered structure of the highly concentrated aqueous dope solution in the gland. This structure was first identified by circular dichroism and infrared spectroscopy of diluted solutions of the dope.[34] Later, NMR spectroscopy studies of dope solutions,[35−37] cast films,[33,38,39] and model peptides[40,41] confirmed the presence of α-helices in the silk gland of *S. c. ricini*. According to these results, the repetitive alanine sequences would adopt this conformation in the gland. Interestingly, common factors such as hydration with aging, mechanical force, and solvent interaction (methanol in particular) were identified as agents capable of inducing an $\alpha \rightarrow \beta$ conformational transition in *S. c. ricini* silk samples. This transition has been observed in the solid state,[39] in solution,[42] and in stretched fibroin fibers.[32,43] In addition, a similar strain-induced conformational transition has been found for fibers of poly(L-alanine),[44] keratin,[45] and hagfish slime.[46] These studies question the universality of the $\alpha \rightarrow \beta$ transition in fibrous proteins and show that further insight is needed to understand the mechanism underlying this phenomenon.

In this work, polarized Raman microspectroscopy has been used to determine the extent of conformational and orientational modifications induced by the mechanical drawing of samples obtained from the spinning dope of the silkworm *S. c. ricini*. A reliable and rational band-fitting procedure has been developed for the amide I band that is composed of strongly overlapping components corresponding to different secondary structures. By using this method, it has been possible to determine the order parameters, $\langle P_2 \rangle$ and $\langle P_4 \rangle$, and to estimate the level of orientation of each secondary structure present in the samples as a function of the draw ratio. In addition, spectra that are only sensitive to conformation, and not to orientation, have been calculated, thus permitting the determination of the content of the different secondary structures. Such quantitative and qualitative information should contribute to a better understanding of the spinning process of silk and improve the production of silk fibers made from recombinant proteins.

Experimental Section

Materials. *S. c. ricini* silkworms were reared in Professor T. Asakura's laboratory (Tokyo University, Japan). The silk glands were excised from fifth instar larvae following a known procedure.[32,43] Each gland was cut and immersed in distilled water. Due to osmotic stress, an insoluble effluent in the shape of a small translucent fibroin ribbon (~0.5 mm in diameter) was expelled from the gland. This gel, referred to as the dope solution, was then cut into smaller pieces with the same initial length. The samples were gently transferred into a diluted acidic solution (acetic acid 0.1%) for 10 min to induce protein coagulation and ensure the removal of any contaminants, such as gland epithelium. The silk fibroin samples were rinsed thoroughly with a potassium chloride solution (1.15%) to remove any traces of acetic acid, and then stretched manually at room temperature to draw ratios (λ) ranging from 0 to 11. To achieve a high level of orientation, tension was applied to the stretched samples to prevent contraction during the drying process, which took place at room temperature during 24 h. Note that the results relative to the fiber stretched at $\lambda = 3$ have been rejected because the experimental data collected for this sample were above standard deviations and clearly deviated with respect to other samples. This might be due to the fact that the stretching could not be totally homogeneous along the fiber. For comparison, degummed[37] *S. c. ricini* cocoon fibers were also analyzed.

Instrumentation. Polarized Raman spectra were obtained using a LabRAM 800HR spectrometer (Horiba Jobin-Yvon, Villeneuve d'Ascq, France) coupled to an Olympus BX 30 fixed stage microscope. The silk samples were mounted onto glass microscope slides using double-sided tape and aligned with the coordinate system used for the orientation measurements (see inset in Figure 5).[31] Spectra were obtained from three acquisitions of 30 s using the 514.5 nm line of an argon laser (Spectra-Physics, model 2020, Mountain View, CA) generating an energy of approximately 2 mW at the sample with a 50× objective (0.75 NA-Olympus). A 100× objective (0.90 NA-Olympus) was used for the cocoon fiber since it has a smaller diameter (~10 μm) compared to that of the fibroin fibers (diameters between 125 and 291 μm). In this configuration, approximately 5 mW was focused on the sample. The confocal hole and the entrance slit of the monochromator were fixed at 200 and 100 μm, respectively. By using a 600 lines/mm holographic grating, it was possible to acquire a spectral window of 1650 cm^{-1} in one exposure (~30 s acquisition time) on a 1-in. open electrode Peltier-cooled CCD detector (1024 × 256 pixels) (Andor Technologies, Belfast, Northern Ireland). Four polarized spectra were obtained in the backscattering configuration for each sample using a half-wave plate and an analyzer respectively placed before and after the sample as described elsewhere.[31] Three series of four polarized spectra were recorded for each λ as well as for the cocoon fiber.

Spectral Treatments. Unless otherwise stated, all data manipulations were performed using GRAMS/AI 7.00 (ThermoGalactic Corporation, Salem, NH). Following the correction for the polarization dependence of the optics in the spectrometer,[31] the spectra were corrected for a small fluorescence background with a polynomial baseline. Thanks to a homemade program run in Mathcad 7 professional (MathSoft Inc.), the three series of spectra were averaged in each polarization after intensity normalization based on the *XX* spectrum and a bandshift offset based on the 1615 cm^{-1} tyrosine band.

Following the work of Frisk et al.,[47] a method has recently been developed in our laboratory to calculate a spectrum that is independent of protein orientation (hereafter called an isotropic spectrum) from the four polarized spectra. The calculation is valid for a uniaxial system and is fully described elsewhere.[48] In the present case, the method was used to generate isotropic spectra of *S. c. ricini* fibroin fibers stretched at different draw ratios to monitor the conformational changes independently of chain orientation.

To quantify the level of orientation of the β-sheets in fibroin fibers, the order parameters $\langle P_2 \rangle$ and $\langle P_4 \rangle$ were calculated following a method previously described.[31] Briefly, this method is based on the determination of two intensity ratios $R_1 = I_{zx}/I_{zz}$ and $R_2 = I_{xz}/I_{xx}$ that can be measured in the backscattering configuration of the Raman microscope. It is only applicable to a vibrational mode for which the Raman tensor (α) is cylindrical in a uniaxial system:

$$\alpha = \begin{pmatrix} \alpha_1 & & \\ & \alpha_1 & \\ & & \alpha_3 \end{pmatrix} = \alpha_3 \begin{pmatrix} a & & \\ & a & \\ & & 1 \end{pmatrix} \text{ with } a = \alpha_1/\alpha_3$$

where α_1 and α_3 are the principal components of the Raman tensor. Since $\langle P_2 \rangle$ and $\langle P_4 \rangle$ are only functions of R_1, R_2, and a (and other parameters that only depend on the objective used), the parameter a has to be determined. This can be done from the value of the depolarization ratio (R_{iso}) of an isotropic (unoriented) sample. In the present case, an isotropic film of *S. c. ricini* fibroin hydrated and then coagulated in a methanol solution (50% v/v) has been used. An average R_{iso} value of 0.20 ± 0.03 was obtained for the β-sheet spectral

component, which is in good agreement with that previously determined for a *Bombyx mori* (*B. mori*) coagulated regenerated film.[31] Finally, from the values of $\langle P_2 \rangle$ and $\langle P_4 \rangle$, and based on the information theory, the most probable distribution of orientation of the β-sheets was determined, $N_{mp}(\theta)$, where θ is the angle with respect to the fiber axis in the uniaxial system (see inset in Figure 5). Details regarding this method can be found in the literature.[31,49,50]

Band Fitting Procedure. Secondary structure contents were evaluated from the amide I band of isotropic spectra. Since it consists of overlapping components due to the different secondary structures present in the sample, curve-fittings of the spectra have been necessary. The decomposition of the polarized spectra further permitted the quantitative determination of the chain orientation of each secondary structure.

The number and position of the components of the experimental spectrum were determined using the following criteria in order of decreasing importance: (i) the minimum number of components; (ii) acknowledged secondary structures present in the considered system; (iii) spectral criteria (shape of the experimental spectra, second derivatives and difference spectra); (iv) generation of a reasonable fit (may require additional bands). In the present case, apart from β-sheets and α-helices that were recognized to be present in the natural fiber and in the spinning dope, respectively, no definitive information was available about other secondary structures. A preliminary investigation (not shown) using the experimental polarized spectra, second derivatives, and difference spectra (calculated with spectra recorded at different λ) has clearly revealed the presence of five amide I components located at 1646, 1657, 1667, 1678, and 1693 cm^{-1} and two other bands at 1597 and 1615 cm^{-1} associated with tyrosine side chains. Another amide I component at 1632 cm^{-1} was found to be essential to keep bandwidths under 22 cm^{-1}. Finally, a very small component at 1710 cm^{-1} was added for a few spectra to obtain reasonable fits.

Before curve-fitting, a linear baseline was subtracted. Band decomposition was performed using Lorentzian−Gaussian band shapes (the percentage of the Lorentzian character is noted %L) on the series of four polarized spectra obtained at different values of λ. It was assumed that the amide I band of all spectra is made of the same set of components, the contribution of each component being different depending on the polarization configuration and λ. Therefore, only variations in intensity between the different spectra were allowed for a given component. In practice, small variations in the position, bandwidth, and %L were tolerated to fit all spectra with the same set of components.

The initial conditions used for the curve-fitting were as follows: the positions were approximately those given above. The bandwidths were arbitrarily fixed at 13 cm^{-1}, except for the components at 1632, 1646, 1678, and 1693 cm^{-1}, which were found to be broader after several preliminary band-fitting attempts. Their bandwidth was then fixed at 15 cm^{-1}. Initial intensities were determined "by eye" such that each manually decomposed spectrum was the closest to the experimental one. The initial value of %L was fixed at 0% for certain components, as determined from preliminary fitting attempts. For components that did not show any clear tendency, a %L of 50% was chosen.

The polarized spectra obtained at $\lambda = 4$ and 10 (a total of eight spectra) were first fitted with the above initial parameters. These two series of spectra were selected since they are representative of the data set, and it was anticipated that, if the fit was successful for both series, it would be also valid for all spectra (a total of 32). During the curve-fitting calculations, all parameters were totally free to evolve. The mean value of a given component parameter calculated over the eight curve-fitted spectra was used as the initial conditions for the second series of curve-fitting calculations on the same spectra. Once again, all parameters were free to evolve. The average values of the resulting parameters were calculated and reinserted in a third series of curve-fittings, but this time, limits were imposed on the parameters. The limits were based on the standard deviation of the parameters calculated from the second band decomposition. The boundaries for the position were ± 0.8 cm^{-1} for the bands at 1693 and 1978 cm^{-1}, and ± 0.5 cm^{-1} for the others. The variations allowed on the bandwidth and %L were ± 1 cm^{-1} and ±15%, respectively.

Finally, the initial conditions and the limits used for the third series of calculations were directly applied to all other polarized and isotropic spectra. All spectra could be well fitted with a total of eight bands in the 1570−1750 cm^{-1} spectral region. The band positions and bandwidths were within ± 0.5 and ± 1 cm^{-1}, respectively, whatever the value of λ. The bandwidth values ranged between 11 and 21 cm^{-1} depending on the component. All bands had a dominant Gaussian character (%L between 0 and 5%) except the bands at 1615 (32−100%), 1657 (26 ± 10%), and 1667 (33 ± 10%) cm^{-1}. The same procedure was also applied to natural silk fibers from three other species (data not presented). It is remarkable that the amide I region of all spectra can be decomposed with similar sets of components (i.e., six amide I components located at similar positions). This rational procedure has allowed us to assess the reliability of the curve-fitting procedure and the uncertainty on the secondary structure contents (±1−2% depending on the component). The content of each secondary structure was calculated from the ratio of the area of a component over the sum of the areas of all the amide I components using the isotropic spectra.

Results and Discussion

Fibroin Conformation: Qualitative Analysis. Figure 1 shows isotropic spectra in different spectral regions at different values of λ. The isotropic spectrum of *S. c. ricini* cocoon silk is also presented for comparison. Region A corresponds to the amide I region, a vibrational mode mainly associated with the stretching of the amide carbonyl groups, sensitive to protein conformation.[51] Since the fibroin fibers were obtained by directly extracting the dope solution from the silkworm glands, the spectrum at $\lambda = 0$ is believed to be representative of the protein native state in the gland. The maximum of the amide I band appears at 1657 cm^{-1}, which is characteristic of the α-helix conformation. This assignment is based on normal-mode calculations and experimental data[51−53] acquired on homopolypeptides, which are good spectroscopic models for proteins.[44] However, the presence of other helical structures, such as 3_1 polyproline helix[53] or 3_1 polyglycine II helix with parallel or antiparallel packing,[51] can also give an amide I band around 1657 cm^{-1}. Nevertheless, the α-helix remains the most probable structure in *S. c. ricini* fibroin since it has been confirmed in the intact gland[35] as well as in the extracted solution.[34,36,37] In addition, the poly(alanine) sequences were found to maintain that structure in the solid state.[33,38,39] Therefore, it can be assumed that the sample at $\lambda = 0$ is representative of the initial content of the gland.

As the draw ratio increases, the α-helical component at 1657 cm^{-1} decreases in intensity, whereas a component at 1667 cm^{-1} becomes progressively predominant. The latter is commonly found in the cocoon silk (Figure 1A) and is assigned to β-sheets. These Raman data clearly show that drawing induces a $\alpha \rightarrow \beta$ conformational transition and that the transition occurs mostly between $\lambda = 4$ and 5, in good agreement with the results obtained by X-ray diffraction, ^{13}C cross polarization/magic-angle spinning (CP/MAS) NMR, and Fourier transform−Raman spectroscopy.[43] Furthermore, the presence of an isosbestic point around 1660 cm^{-1} reveals, for the first time, that the transition is a two-state process. Similar features were also observed on the polarized spectra.

Figure 1B shows the amide III region, which is also sensitive to protein conformation. This coupled vibrational mode is mainly due to the NH bending and the H^{α} bending vibrations. At $\lambda = 0$, the amide III band is dominated by a component at

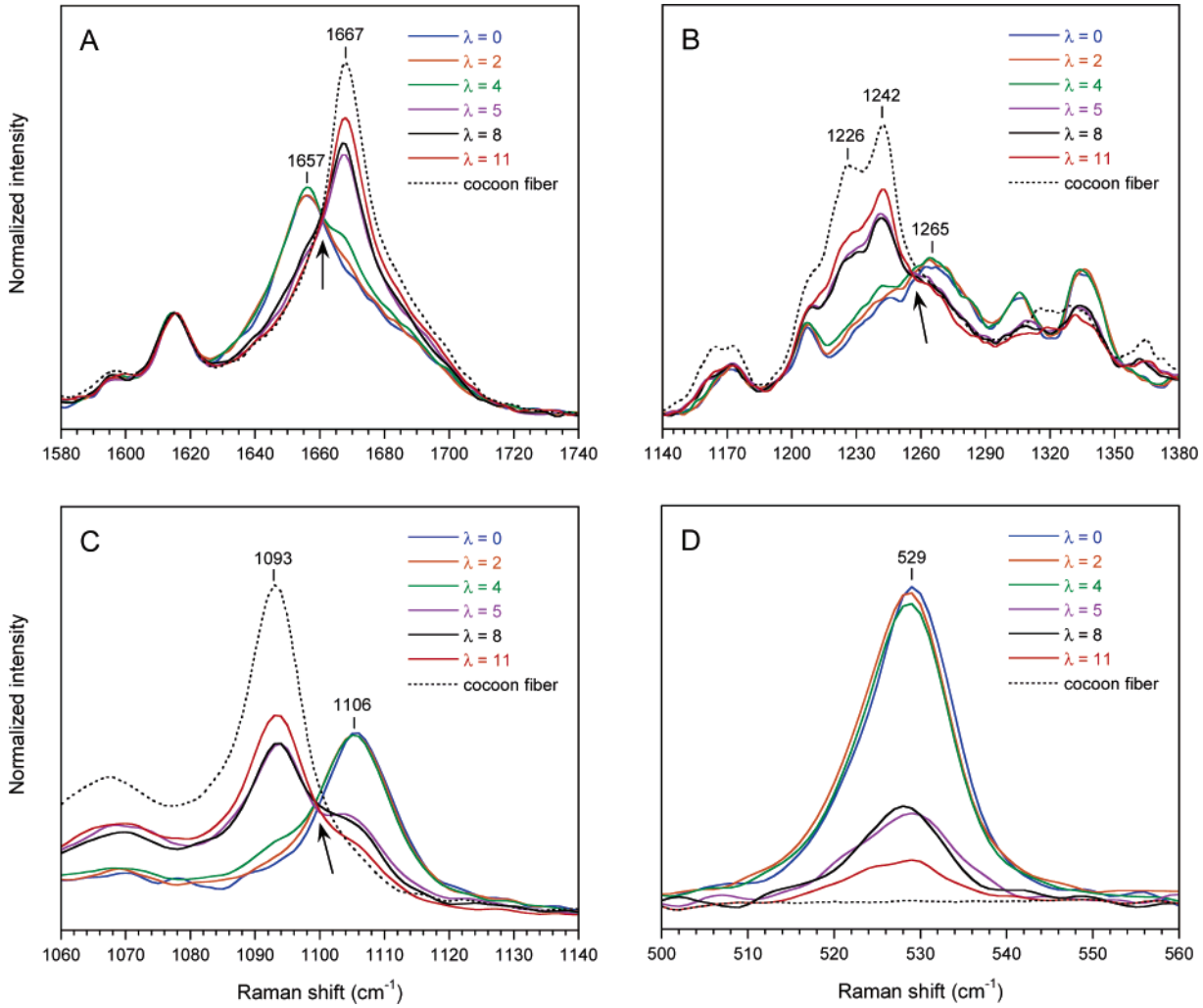

Figure 1. Effect of the draw ratio on the isotropic spectra of *S. c. ricini* fibroin fibers in four different spectral regions. The spectrum of cocoon silk is added for comparison. (A) Amide I [1580−1740 cm^{-1}]; (B) Amide III [1140−1380 cm^{-1}]; (C) $C^{\alpha}-C^{\beta}$ stretching and side chains [1060−1140 cm^{-1}]; (D) Helices' spectral footprint [500−560 cm^{-1}]. The isosbestic points are marked by black arrows.

1265 cm^{-1} assigned to the α-helical conformation since a similar component was found at 1261 cm^{-1} in the Raman spectrum of α-poly(L-alanine).[51,52] When λ increases, two components at 1242 and 1226 cm^{-1} strongly increase in intensity. These two bands are associated with the β-sheet conformation adopted by the poly(L-alanine) sequences and are assigned to the amide III modes with A and B_1 symmetry, respectively.[51] The polarization dependence of these two modes for cocoon silk have been discussed in a previous study.[31] As in the amide I region, an isosbestic point is observed near 1260 cm^{-1}, thus confirming the two-state process taking place upon mechanical deformation.

Figure 1C is characteristic of the $C^{\alpha}-C^{\beta}$ stretching region. Upon mechanical deformation, a band at 1106 cm^{-1} decreases in intensity at the expense of a band at 1093 cm^{-1}, and an isosbestic point appears around 1100 cm^{-1}. These two bands are due to coupled vibrational modes involving the $C^{\alpha}-C^{\beta}$ stretching and the CH_3 rocking vibrations.[51] According to our data, these vibrational modes are sensitive to protein conformation, like amide vibrations. The 1106 cm^{-1} band has previously been assigned to poly(alanine) in the α-helical conformation.[44,51−53] The band at 1093 cm^{-1} has been assigned to a C−C stretching mode of the protein backbone in the disordered conformation in cocoon silk.[54] However, our results show clearly that the intensity of this band increases with increasing strain and that it is due to β-sheets, as observed in β-poly(alanine).[51] Moreover, a bandshift from 1106 to 1093 cm^{-1} has also been observed when cast films prepared from either *S. c. ricini* (unpublished data) or *Antheraea pernyi* (*A. pernyi*)[55,56] dope solutions are immersed in methanol or ethanol solutions, solvents that are recognized to favor the formation of β-sheets. Note that the primary sequence of *A. pernyi* cocoon silk is similar to that of *S. c. ricini*.[57,58] These results undoubtedly confirm that the bands at 1106 and 1093 cm^{-1} are conformation sensitive.

Figure 1D shows a band at 529 cm^{-1} whose intensity decreases with increasing draw ratio. This band is characteristic of α-poly(alanine)[52,53] and arises from the contribution of several vibrational modes, including the carbonyl in plane bending, the $C^{\alpha}-C-N$ deformation, and the $C^{\alpha}-C$ stretching vibrations.[51] It becomes very weak as the β-sheet conformation becomes the dominant structure at draw ratios higher than 4. Interestingly, the band at 529 cm^{-1} is still visible at $\lambda = 11$, while it is totally absent in the cocoon fiber spectrum. Consequently, it appears that a small amount of α-helices still remains, even for high draw ratios. The fact that such a band has not been observed in the Raman spectra of other α-helical polypeptides, such as poly-γ-benzyl-L-glutamate and poly-L-leucine,[53] indicates that it is associated with repetitive alanine sequences that are long enough to adopt the α-helix structure. The presence of this band demonstrates unambiguously that alanine sequences predominantly adopt the α-helix structure in the fibroin, and are thus

representative of the spinning dope ($\lambda = 0$), as well as in samples with a draw ratio smaller than 5. This result is in agreement with the high-resolution solid-state NMR measurements obtained on specifically labeled alanine residues.[33,39] This finding is not surprising since, among all natural amino acids, alanine has the highest helical propensity.[59] Studies of poly(alanine) peptides have indeed demonstrated that the α-helix is the dominant secondary structure adopted in water by alanine sequences in polypeptides as short as 13 residues,[60,61] while the helical structure was not observed for sequences shorter than 10 residues.[62] Thus, the length of the alanine sequences found in *S. c. ricini* (10−13 residues) would be responsible for the predominance of helical structures in the dope solution. On the contrary, Hronska et al.[63] have shown by NMR spectroscopy that the proteins in a *N. edulis* intact gland, which contains shorter alanine sequences, does not have a well-defined secondary structure.

Fibroin Conformation: Quantitative Analysis. As seen in Figure 1A, the spectra of silk fibroins in the amide I region consist of the superposition of bands since the fibroin conformation is a mixture of secondary structures with various dihedral angles and hydrogen bonding patterns. Nevertheless, Figure 1A clearly shows that the spectra associated with the initial and final states are dominated by the α-helix or β-sheet contributions, respectively. This series of spectra represents an excellent set of data to adequately decompose the amide I region in its different overlapping components. To quantitatively determine the different secondary structures, we have developed a method to calculate an isotropic spectrum and a band decomposition procedure of the amide I band, as described in the Experimental Section.

Typical curve-fittings obtained at three representative draw ratios ($\lambda = 0$, 4, and 11) are presented in Figure 2. The amide I band was decomposed using six components. As discussed above, the bands at 1657 and 1667 cm^{-1} are assigned to the α-helix and β-sheet conformations, respectively. The assignment of the components at 1693, 1678, and 1646 cm^{-1} is less straightforward. From normal-mode analysis of polypeptides, the position of the amide I band of β-turns has been found to arise over a wide range of wavenumbers.[64] Considering a transition dipole coupling, $\Delta\mu_{eff}$ (effective dipole moment), between 0.35 and 0.45 D for the amide I mode of turns,[65] three amide I wavenumber domains due to peptide bonds in type I and type III β-turns were found at 1690−1702, 1679−1686, and 1640−1648 cm^{-1}. These spectral regions correspond remarkably well to the three components found by band decomposition at 1693, 1678, and 1646 cm^{-1}. Therefore, these components are assigned to turns, most probably to type I and type III β-turns, as the wavenumbers of type II β-turns do not match the position of the observed components very well.[65] Furthermore, distorted turns[64] are likely to be present since the components at 1693, 1678, and 1646 cm^{-1} are relatively broad (bandwidths of 21.4 ± 0.8, 17.8 ± 0.7, and 17.2 ± 0.6 cm^{-1}, respectively) compared to the β-sheet (13.2 ± 0.7 cm^{-1}) and α-helix (13.6 ± 0.8 cm^{-1}) components. These bandwidths are consistent with the fact that the position of the vibrational modes assigned to the turns depends on the dihedral angles.[66] The assignment of the 1632 cm^{-1} component is unclear at present. It can be due to turns,[64] β-sheets, or unordered structures.[67] This component accounts for only 5% of the total area of the amide I band, a proportion that remains approximately constant for all λ (±1%). The small component at 1710 cm^{-1} may be due to the C═O stretching vibration of glutamine and arginine residues. The two bands at 1597 and 1615 cm^{-1} are both assigned to vibrations of the aromatic amino acids, including the tyrosine side chains.[68]

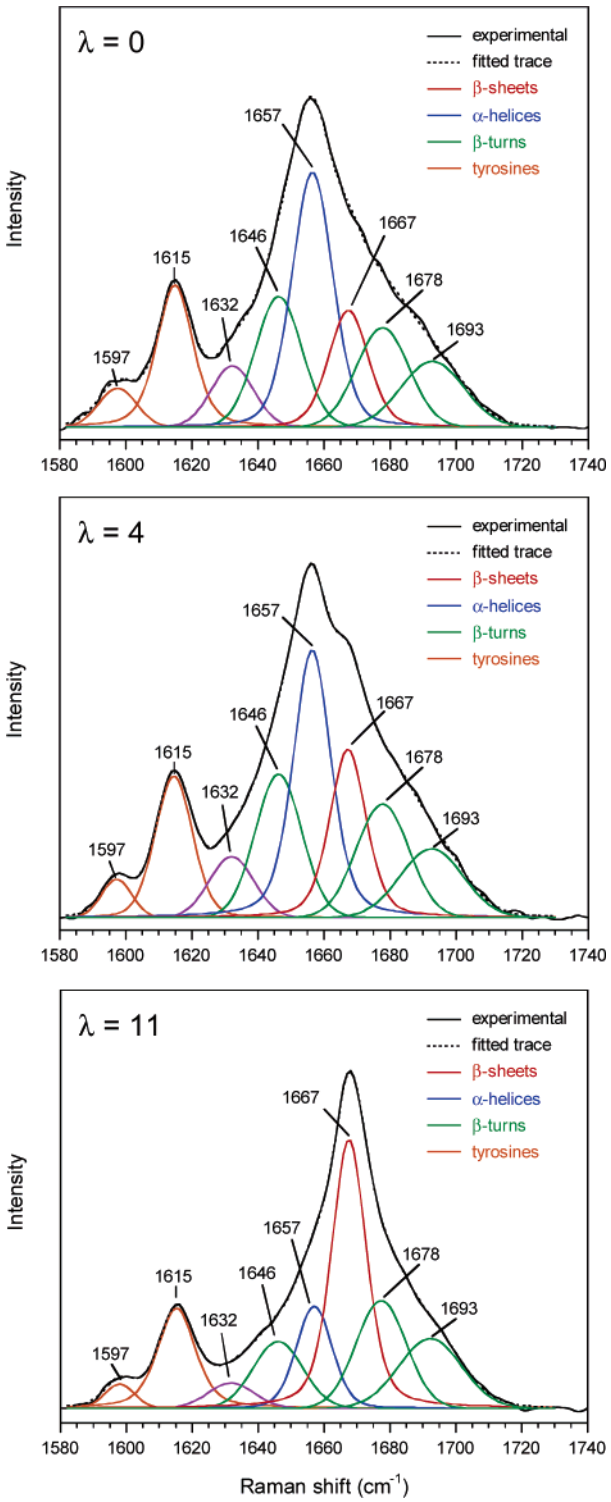

Figure 2. Band decomposition of the amide I region [1580−1740 cm^{-1}] of the isotropic spectra for three different draw ratios.

Figure 2 clearly illustrates the strong contribution of the α-helix and β-sheet components in the initial ($\lambda = 0$) and final ($\lambda = 11$) states, respectively. The intermediate state ($\lambda = 4$) shows a mixture of both structures, with a higher helical content. From these decomposed spectra, the proportion of the components due to the α-helices, β-sheets, and the sum of the other secondary structures as a function of λ was calculated, and the results obtained are presented in Figure 3. As seen in this figure,

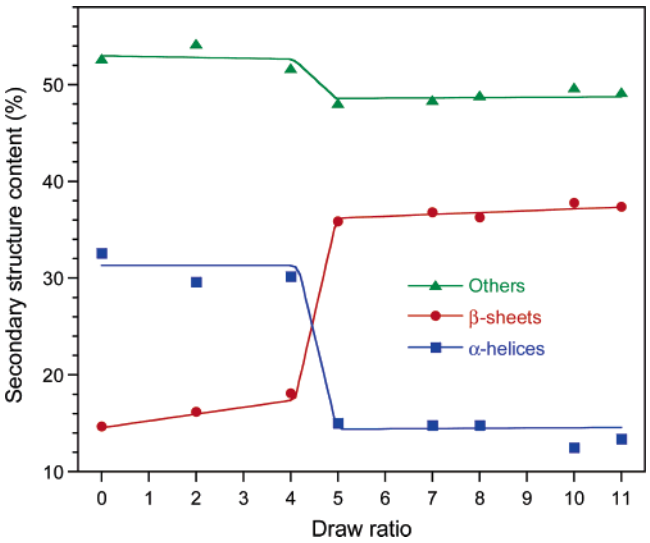

Figure 3. Secondary structure content as a function of draw ratio in stretched fibroin fibers. The proportion of each secondary structure (others, α-helices and β-sheets) was obtained from the area under the band associated to each spectral component as determined by the band decomposition method illustrated in Figure 2. The lines shown are only a guide to the eye.

the helical content is 33 ± 2% at $\lambda = 0$, which is slightly higher than the value of 25 ± 2% found by ^{13}C NMR measurements.[69,70] From the primary sequence of *S. c. ricini* fibroin, 40% of the amino acids are found in the alanine repeats. Since α-helices are primarily formed by the alanine repetitive sequences, our results suggest that ~82% of these alanines are involved in α-helices in the spinning dope, while a percentage of 65−70% has been estimated by Kimura et al. from peak intensity ratios in solid-state NMR spectra.[35] Upon stretching, the helical content decreases, especially between $\lambda = 4$ and 5, and finally reaches 13 ± 2% at $\lambda = 11$. This result is consistent with the fact that the band due to the α-helical structure at 529 cm^{-1} is still present at high draw ratios (Figure 1D).

Figure 3 clearly shows that, in parallel with the loss of α-helical structure, there is an increase in the amount of the β-sheets. Interestingly, the major conformational changes occur over a narrow draw ratio interval, between 4 and 5, and the sigmoid-like curve reveals that the conformational transition is cooperative. Moreover, the fact that the onset of the transition occurs at $\lambda = 4$, as observed previously by ^{13}C CP/MAS NMR spectroscopy for *S. c. ricini* fibroin fibers drawn using a motorized stretcher,[43] strongly suggests that the α → β transition occurs at a critical draw ratio. The initial state contains approximately 15 ± 2% of β-sheets, a proportion that reaches 37 ± 2% at $\lambda = 11$. Therefore, the increase in the β-sheet content (22%) is slightly higher than the decrease in the α-helical content (20%). A slight decrease in the proportion of the other secondary structures indicates that amino acids that initially adopt a nonhelical structure are incorporated into the β-sheets after the conformational transition. The glycine−glycine motif found near both ends of the repetitive alanine sequence (observed 72% of the time in the *S. c. ricini* primary sequence)[28] could be involved in this conformational change. The spectral changes due to these residues is, however, not large enough to preclude the observation of the isosbestic points within the experimental error.

The proportion of β-sheets at $\lambda = 11$ represents 92% of the residues that belong to the alanine repeats of the fibroin primary structure. This indicates that not all the residues that are thought to be involved in β-sheets in the cocoon fiber actually form β-sheets in the stretched fibroin fibers. Recent results in our laboratory using the same band fitting procedure (results not presented) have shown that the proportion of β-sheets in *S. c. ricini* cocoon fiber is 47 ± 2%. Similarly, Yang et al. also found a smaller fraction of β-sheets in stretched fibroin fiber ($\lambda = 10$) compared to cocoon fiber using NMR spectroscopy.[43] Since a draw ratio of 11 is rather unlikely in nature, these results suggest that additional factors, other than stretching, contribute to optimize the amount of β-sheet in natural cocoon silk.

Fibroin Orientation: Quantitative Analysis. We have recently developed a method to quantify the level of molecular orientation using Raman microspectroscopy.[31] This method is based on the measurement of the intensity of the four polarized spectra in the amide I region and has been applied to silk samples to determine the orientation of the β-sheets. Since the β-sheet component dominates the amide I band in cocoon silk (similar to the spectra in *XX* for $\lambda = 11$), the peak height of the amide I band was used as a first approximation.[31] The band decomposition procedure developed in this work has allowed us to determine the level of orientation of the different secondary structures using the intensity of the pure components obtained from the spectral decomposition of the polarized spectra. Figure 4 shows a typical example of the band decomposition for the four polarized spectra at $\lambda = 11$. For the *XX* polarization, the β-sheet component clearly dominates the amide I band, while an approximately equal amount of both α-helices and β-sheets appears in the crossed-polarized spectra (I_{XZ} and I_{ZX}). As can be seen, the four polarized spectra of an oriented fibroin fiber are different in shape, but they can be reproduced with the same set of spectral components, which validates the band decomposition model proposed.

The method used to determine the orientation is only applicable for a Raman tensor showing a cylindrical symmetry[31] and also requires that the value of R_{iso} obtained from an isotropic sample is known. This has been possible for the β-sheet spectral component by using an isotropic coagulated film (unoriented) obtained by casting the liquid silk extracted from *S. c. ricini* gland (see Experimental Section). The intensity ratios R_1 and R_2 (see Experimental Section) for the β-sheet component at 1667 cm^{-1}, and the order parameters $\langle P_2 \rangle$ and $\langle P_4 \rangle$ calculated from these ratios are given in Table 1. As can be seen, the negative value of $\langle P_2 \rangle$ decreases considerably between $\lambda = 4$ and $\lambda = 5$, that is, at the same draw ratio where major conformational changes occur (Figure 3). These results reveal that the abrupt conversion of the α-helical structure and the significant increase in the level of orientation of the β-sheets in response to the applied strain are concomitant phenomena. The fact that the $\langle P_2 \rangle$ values determined for $\lambda \leq 4$ are all close to zero, within the experimental error, indicates that the β-sheets are isotropically distributed. As soon as the β-sheets become the dominant structure at $\lambda \geq 5$, $\langle P_2 \rangle$ rapidly decreases to −0.28 and reaches −0.37 at $\lambda = 11$. The latter result reveals that the amide carbonyl groups are highly oriented perpendicularly to the fiber axis since the theoretical limiting value of $\langle P_2 \rangle$ is equal to −0.5 for a perfect perpendicular orientation. Previous X-ray measurements have indicated the presence of an oriented pattern of β-sheets in *S. c. ricini* fibroin fiber stretched six times ($\lambda = 6$).[43] Most of the stretched fibroin fibers show that the orientation of the β-sheets increases with strain. On the basis of the fit of the amide I band, the $\langle P_2 \rangle$ and $\langle P_4 \rangle$ couples calculated are (−0.37; 0.23) and (−0.41; 0.23) for the most stretched fibroin sample and cocoon silk, respectively. Thus, even for the most stretched sample, the level of orientation of the β-sheets is not as high as that of cocoon silk. It is interesting to note here that the values

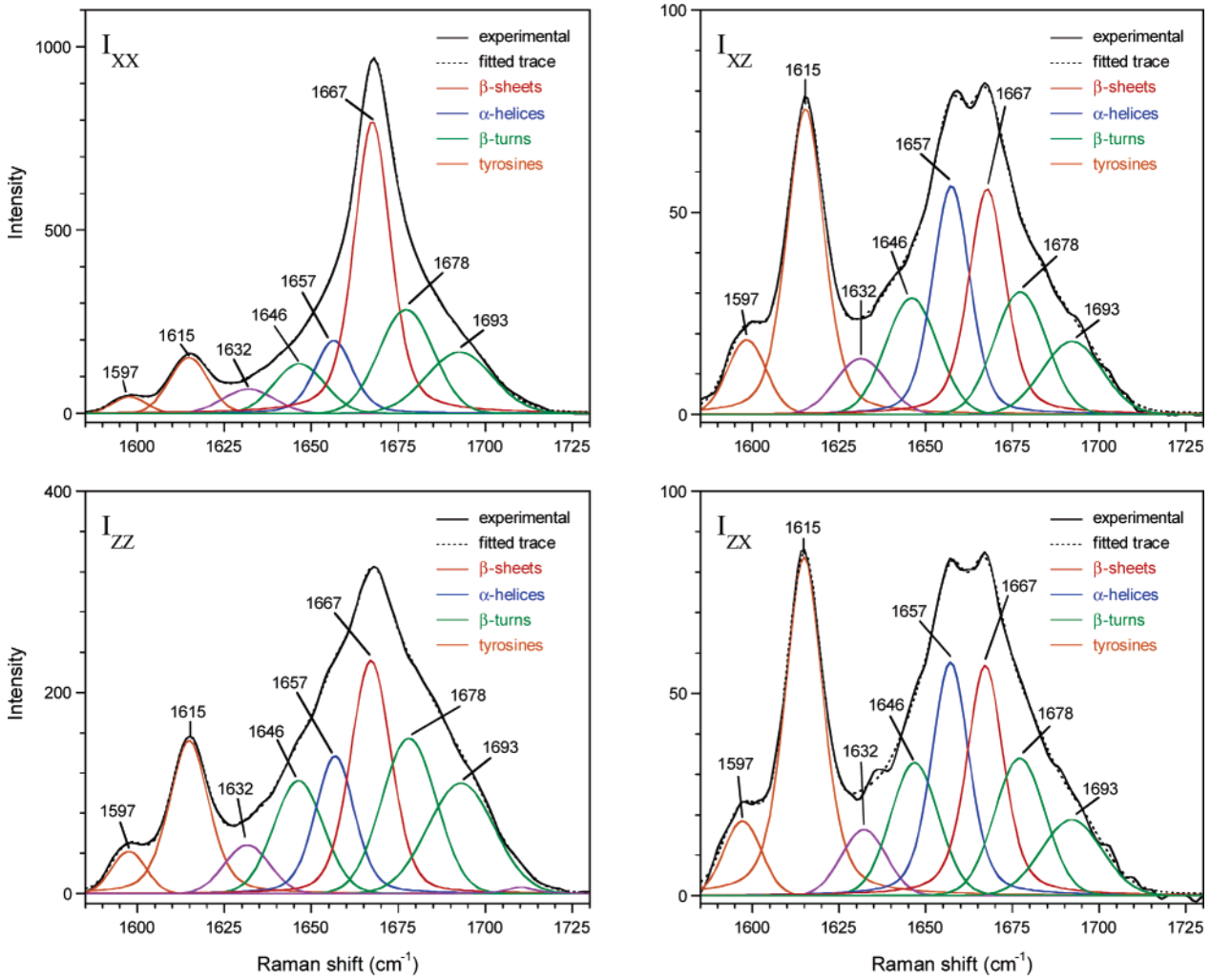

Figure 4. Band decomposition of the amide I region of the polarized Raman spectra obtained for the draw ratio of 11 for the four polarizations.

Table 1. Intensity Ratios, R_1 and R_2, and Order Parameters, $\langle P_2 \rangle$ and $\langle P_4 \rangle$, for the β-Sheet Amide I Band for Fibroin Fibers Stretched at Different Draw Ratios

	β-sheet band at 1667 cm^{-1}			
	$R_1 = I_{ZX}/I_{ZZ}$	$R_2 = I_{XZ}/I_{XX}$	$\langle P_2 \rangle$	$\langle P_4 \rangle$
draw ratio	±0.01	±0.01	±0.02	±0.02
0	0.21	0.21	0.01	0.00
2	0.21	0.20	−0.03	0.02
4	0.22	0.19	−0.05	0.01
5	0.25	0.10	−0.28	0.14
7	0.30	0.07	−0.38	0.21
8	0.26	0.09	−0.33	0.19
10	0.25	0.08	−0.33	0.19
11	0.25	0.07	−0.37	0.23
cocoon fiber	0.26	0.08	−0.41	0.23

determined for the cocoon silk fiber after band decomposition are slightly lower than those obtained previously (−0.36; 0.19)[31] by using the peak height intensity of the amide I band. This is mainly due to overlapping contributions from other less oriented conformations such as helices and turns when the peak height is used.

Figure 5 shows the effect of the draw ratio on the most probable orientation distribution function $N_{mp}(\theta)$ calculated from the $\langle P_2 \rangle$ and $\langle P_4 \rangle$ values.[31] For $\lambda < 4$, $N_{mp}(\theta)$ is almost constant for all values of θ, which is characteristic of an isotropic system. Above $\lambda = 4$, the distribution of orientation is characterized by

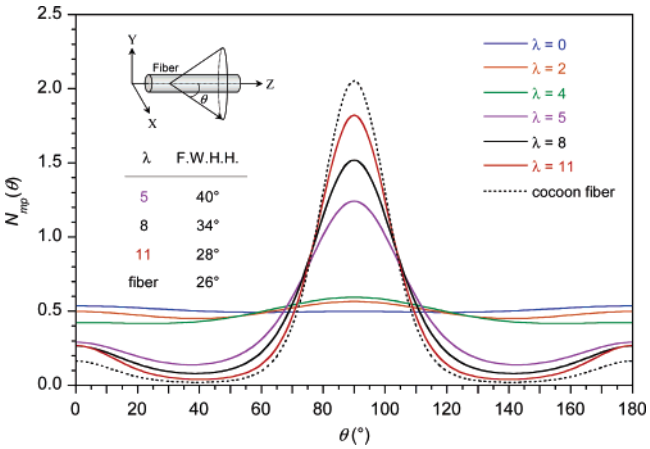

Figure 5. Effect of the draw ratio on the most probable orientation distribution function of the β-sheets in stretched *S. c. ricini* fibroin fibers. The width of the distribution is listed in the inset for the different draw ratios.

an unimodal, nearly Gaussian distribution centered at 90°, which shows that the C═O bonds in β-sheets are preferentially oriented perpendicular to the fiber axis. The distribution becomes narrower as λ increases, showing that the orientation level increases. At $\lambda = 11$, $N_{mp}(\theta)$ is close to that calculated for *S. c. ricini* cocoon silk fiber,[31] but, as seen in the inset table in Figure 5, the width of the distribution is 28° at $\lambda = 11$ and 26° for cocoon silk. This result indicates that the alignment of the

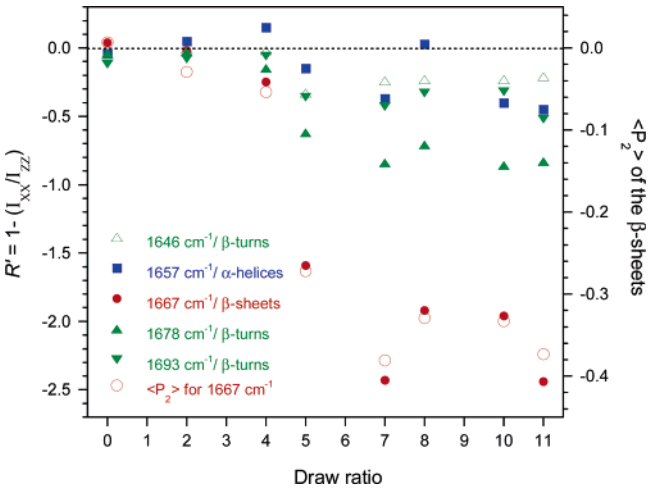

Figure 6. Semiquantitative order parameter (R') as a function of the draw ratio for the different amide I components shown in Figure 2. The order parameter $\langle P_2 \rangle$ determined for the β-sheet component is superimposed for comparison.

carbonyl groups in cocoon silk is better than that of the most stretched fibroin fiber. NMR detailed structural analyses have indicated that 75% of the total alanine residues were confined in oriented regions in a fibroin sample stretched 10 times ($\lambda = 10$).[32]

Even though our results show that the β-sheet content and level of orientation of these β-sheets could be quite high in stretched fibroin fibers, it is unlikely that the silkworm is able to achieve a draw ratio of 11 from the mechanical strain on the silk thread induced by its head and body motions while spinning. Other factors such as extensional flow and shear forces occurring in the spinning duct, protein concentration changes leading to the formation of a liquid crystalline phase that facilitates the prealignment of the molecular chains, the interaction of specific ions, and pH changes along the spinning apparatus should have significant effects on the final β-sheet alignment within the fiber.[17] In addition, it has been shown by shear forces measurements that sericin, a protein embedding the fibroin fibers to form the final cocoon thread, plays an important role in the nucleation of β-sheets in the anterior portion of the silk gland.[71]

Attempts to determine the order parameters of secondary structures other than β-sheets using the decomposed spectra have not been successful because the depolarization ratio R_{iso} (see Experimental Section) could not be appropriately determined either for the α-helices or for the β-turns. It seems that the error on the band decomposition method may be too large to precisely represent the small dichroic changes that occur for turns or helices. Therefore, to determine the level of orientation of all secondary structures, the pseudo-order parameter $R' = 1 - (I_{XX}/I_{ZZ})$ proposed by Frisk et al. has been used.[47] Like $\langle P_2 \rangle$, this order parameter is equal to 0 for an isotropic orientation, is equal to 1 for perfect parallel orientation, and is negative for perpendicular orientation. However, it can reach values lower than −0.5. Figure 6 shows the values of R' calculated for the different amide I band components as a function of λ. For clarity, the band at 1632 cm^{-1} was omitted since it does not show any preferential orientation. As can be seen, R' is close to 0 for $\lambda \leq 4$, showing that all the secondary structures are unoriented. For $\lambda \geq 5$, the values of R' are all negative, indicating that the intensity of the corresponding Raman band is higher in the *XX* than in the *ZZ* polarization. Thus, the amide carbonyl groups of all secondary structures are predominantly aligned toward the *X* axis, that is, perpendicular to the fiber axis. Therefore, the polypeptide chains are preferentially aligned along the fiber axis in the stretched fibers. As expected, the β-sheets show the highest level of orientation among all structures. For comparison, the $\langle P_2 \rangle$ values reported in Table 1 are also included in Figure 6. The obvious correlation between R' and $\langle P_2 \rangle$ for all values of λ reveals that the former, although it is not a truly quantitative parameter, permits the semiquantitative characterization of the orientation level. Surprisingly, the α-helices are barely or not oriented at all λ values. One would have expected to find partially oriented α-helices upon drawing. For example, in natural wool fiber (which is essentially pure keratin proteins), α-helices are mainly oriented parallel to the fiber axis[72] and undergo an $\alpha \rightarrow \beta$ conformational transition when cast films[73,74] or single fibers[45,75] are stretched. On the other hand, our results indicate that, as soon as the α-helices in *S. c. ricini* fibroin fibers are subjected to sufficient strain, they are converted into oriented β-sheets without any noticeable orientation of the helices. The fact that the α-helices do not orient toward the stretching direction indicates that the β-sheet structure is more stable than α-helices in silk samples. This finding suggests that, whereas α-helix is the preferred conformation to keep the proteins in solution in an unoriented state at high concentration in the aqueous dope, β-sheet structure is favored in the final silk threads.

As judged from the negative value of R', the β-turns seem to be slightly oriented. Therefore, not only are β-sheets aligned along the fiber axis, but the glycine-rich domains of the fibroin where the turns are mainly located also appear to be partly oriented. The turn component at 1678 cm^{-1} has the more negative value of R', which suggests that this vibrational mode might be associated with turns that are adjacent to β-sheets, that is, turn segments that connect two β-strands. According to normal-mode calculations, this mode in type I and III β-turns would be localized on the carbonyl of the first peptide group at the end of the sheet structure.[51]

Recently, the effect of drawing on wet-spun regenerated *B. mori* fibroin fiber has been investigated. The fiber's tenacity was greatly improved with increasing draw ratio and was attributed to molecular orientation.[27] This finding supports the fact that it is of prime importance to be able to adequately characterize protein conformation and chain orientation to improve our knowledge of the structure−property relationships that can then help the processing of recombinant silk fibers.

Conclusion

Our results show that the *S. c. ricini* fibroin fibers prepared from the spinning dope undergo a cooperative conformational transition under the application of a mechanical deformation, in agreement with previous results.[43] The proteins, in particular the alanine sequences, mainly adopt the α-helix conformation in the gland (33 ± 2%) and are converted to β-sheets upon stretching (37 ± 2%). Our results indicate that the transition occurs above the critical draw ratio of 4. Although this transition can be described as a two-state process, our results suggest that part of the glycine residues might be incorporated into β-poly(alanine) structures. The quantification of the secondary structures highlights the fact that a lower content of β-sheet is achieved by stretching (at $\lambda = 11$) compared to cocoon fibroin fiber. This finding confirms that strain is not the only physical parameter that generates β-sheet structure in silk fibroin. In addition, the β-sheets were found to have a higher level of orientation in cocoon silk, although a relatively narrow orientation distribution was obtained for high elongation ratios. This can be related to the mechanical properties that are superior for the cocoon silk.

The conformational transition occurring in stretched *S. c. ricini* fibroin fibers has been found to be a particularly interesting system for the development of a curve-fitting procedure for the amide I band. The band decomposition parameters have been validated on polarized and isotropic spectra, and the method has been successfully applied to Raman spectra obtained for other types of silk having different amino acid sequences (data not shown).

For the first time, the level of orientation of the different secondary structure elements present in *S. c. ricini* samples could be quantified by polarized Raman spectroscopy. The determination of the pseudo-order parameter R' for all components of the amide I band reveals that the α-helices are neither oriented in the initial state nor oriented when subjected to mechanical deformation. On the other hand, β-sheet structures reach a high degree of orientation after $\lambda = 5$. Interestingly, the increase in the orientation level of the β-sheets is concomitant with the α $\rightarrow \beta$ conformational conversion. Spectral components associated with β-turns show a slight level of orientation, somewhat lower than that observed for β-sheets. The results suggest that part of the turns are close in space to highly oriented β-sheets. Since all spectral components give negative R' values, most of the carbonyls, independently of the adopted conformation, seem to be mainly perpendicular to the fiber axis.

The $\langle P_2 \rangle$ and $\langle P_4 \rangle$ order parameters determined for the β-sheets show that, at high strain, a high level of orientation is obtained, but lower than that of cocoon silk. The spectral signature of the α-helices at 529 cm^{-1} is still visible on the spectrum obtained for the highest elongation ratio ($\lambda = 11$), indicating that a small amount of helical conformation is still present for the stretched fibers while it is absent in the cocoon silk spectrum.

Acknowledgment. Funding for the Raman microspectrometer was made possible through a grant from the Canadian Foundation for Innovation. This work was also supported by grants from the Natural Sciences and Engineering Research Council (NSERC) of Canada and the Fonds Québécois de Recherche sur la Nature et les Technologies (FQRNT). T.A. acknowledges support from the Insect Technology Project and Asahi Glass Foundation in Japan. Graduate scholarships from NSERC (M.-E.R.), FQRNT (M.-E.R. and L.B.), and the Fondation de l'Université Laval (M.-E.R.) as well as an undergraduate NSERC scholarship to J.P. are also acknowledged. The authors express their thanks to Serge Groleau and François Lapointe for their technical support.

References and Notes

(1) Kaplan, D. L. *Polym. Degrad. Stab.* **1998**, *59*, 25−32.
(2) Gosline, J.; Lillie, M.; Carrington, E.; Guerette, P.; Ortlepp, C.; Savage, K. *Philos. Trans. R. Soc. London, Ser. B* **2002**, *357*, 121−132.
(3) Viney, C.; Bell, F. *Curr. Opin. Solid State Mater. Sci.* **2004**, *8*, 165−171.
(4) O'Brien, J. P.; Fahnestock, S. R.; Termonia, Y.; Gardner, K. H. *Adv. Mater.* **1998**, *10*, 1185−1195.
(5) Gührsa, K. H.; Weisshart, K.; Grosse, F. *J. Biotechnol.* **2000**, *74*, 121−134.
(6) Fahnestock, S. R.; Yao, Z.; Bedzyk, L. A. *J. Biotechnol.* **2000**, *74*, 105−119.
(7) Scheller, J.; Gührs, K. H.; Grosse, F.; Conrad, U. *Nat. Biotechnol.* **2001**, *19*, 573−577.
(8) Lazaris, A.; Arcidiacono, S.; Huang, Y.; Zhou, J.-F.; Duguay, F.; Chretien, N.; Welsh, E. A.; Soares, J. W.; Karatzas, C. N. *Science* **2002**, *295*, 472−476.
(9) Yang, J.; Barr, L. A.; Fahnestock, S. R.; Liu, Z.-B. *Transgenic Res.* **2005**, *14*, 313−324.
(10) Scheibel, T. *Microb. Cell Fact.* **2004**, *3*, 1−14.
(11) Vollrath, F. *Rev. Mol. Biotechnol.* **2000**, *74*, 67−83.
(12) Viney, C. *Curr. Opin. Struct. Biol.* **2004**, *8*, 95−101.
(13) Valluzzi, R.; Winkler, S.; Wilson, D.; Kaplan, D. L. *Philos. Trans. R. Soc. London, Ser. B* **2002**, *357*, 165−167.
(14) Huemmerich, D.; Scheibel, T.; Vollrath, F.; Cohen, S.; Gat, U.; Ittah, S. *Curr. Biol.* **2004**, *14*, 2070−2074.
(15) Magoshi, J.; Magoshi, Y.; Nakamura, S. Silk Polymers. *ACS Symp. Ser.* **1994**, *544*, 292−310.
(16) Knight, D. P.; Vollrath, F. *Naturwissenschaften* **2001**, *88*, 179−182.
(17) Vollrath, F.; Knight, D. P. *Nature* **2001**, *410*, 541−548.
(18) Foo, C. W. P.; Bini, E.; Hensman, J.; Knight, D. P.; Lewis, R. V.; Kaplan, D. L. *Appl. Phys. A: Mater. Sci. Process.* **2006**, *82*, 223−233.
(19) Kerkam, K.; Viney, C.; Kaplan, D.; Lombardi, S. *Nature* **1991**, *349*, 596−598.
(20) Willcox, P. J.; Gido, S. P.; Muller, W.; Kaplan, D. L. *Macromolecules* **1996**, *29*, 5106−5110.
(21) Knight, D.; Vollrath, F. *Philos. Trans. R. Soc. London, Ser. B* **2002**, *357*, 155−163.
(22) Trabbic, K. A.; Yager, P. *Macromolecules* **1998**, *31*, 462−471.
(23) Liivak, O.; Blye, A.; Shah, N.; Jelinski, L. W. *Macromolecules* **1998**, *31*, 2947−2951.
(24) Seidel, A.; Liivak, O.; Calve, S.; Adaska, J.; Ji, G.; Yang, Z.; Grubb, D.; Zax, D. B.; Jelinski, L. W. *Macromolecules* **2000**, *33*, 775−780.
(25) Arcidiacono, S.; Mello, C. M.; Butler, M.; Welsh, E.; Soares, J. W.; Allen, A.; Ziegler, D.; Laue, T.; Chase, S. *Macromolecules* **2002**, *35*, 1262−1266.
(26) Shao, Z.; Vollrath, F.; Yang, Y.; Thogersen, H. *Macromolecules* **2003**, *36*, 1157−1161.
(27) Um, I.; Ki, C.; Kweon, H.; Lee, K.; Ihm, D.; Park, Y. *Int. J. Biol. Macromol.* **2004**, *34*, 107−119.
(28) Yukuhiro, K. National Institute of Agrobiological Sciences, Tsukuba, Japan, personal communication, 2002.
(29) Xu, M.; Lewis, R. V. *Proc. Natl. Acad. Sci. U.S.A.* **1990**, *87*, 7120−7124.
(30) Hinman, M. B.; Lewis, R. V. *J. Biol. Chem.* **1992**, *267*, 19320−19324.
(31) Rousseau, M.-E.; Lefevre, T.; Beaulieu, L.; Asakura, T.; Pezolet, M. *Biomacromolecules* **2004**, *5*, 2247−2257.
(32) Asakura, T.; Ito, T.; Okudaira, M.; Kameda, T. *Macromolecules* **1999**, *32*, 4940−4946.
(33) van Beek, J. D.; Beaulieu, L.; Schafer, H.; Demura, M.; Asakura, T.; Meier, B. H. *Nature* **2000**, *405*, 1077−1079.
(34) Iizuka, E. *Biochim. Biophys. Acta* **1968**, *160*, 454−463.
(35) Asakura, T.; Suzuki, H.; Watanabe, Y. *Macromolecules* **1983**, *16*, 1024−1026.
(36) Asakura, T.; Tanaka, C.; Yang, M.; Yao, J.; Kurokawa, M. *Biomaterials* **2004**, *25*, 617−624.
(37) Asakura, T.; Kashiba, H.; Yoshimizu, H. *Macromolecules* **1988**, *21*, 644−648.
(38) Saitô, H.; Tabeta, R.; Asakura, T.; Iwanaga, Y.; Shoji, A.; Ozaki, T.; Ando, I. *Macromolecules* **1984**, *17*, 1405−1412.
(39) Ishida, M.; Asakura, T.; Yokoi, M.; Saitô, H. *Macromolecules* **1990**, *23*, 88−94.
(40) Nakazawa, Y.; Bamba, M.; Nishio, S.; Asakura, T. *Protein Sci.* **2003**, *12*, 666−671.
(41) Nakazawa, Y.; Asakura, T. *J. Am. Chem. Soc.* **2003**, *125*, 7230−7237.
(42) Nakazawa, Y.; Nakai, T.; Kameda, T.; Asakura, T. *Chem. Phys. Lett.* **1999**, *311*, 362−366.
(43) Yang, M.; Yao, J.; Sonoyama, M.; Asakura, T. *Macromolecules* **2004**, *37*, 3497−3504.
(44) Frushour, B. G.; Koenig, J. L. *Biopolymers* **1974**, *13*, 455−474.
(45) Kreplak, L.; Doucet, J.; Dumas, P.; Briki, F. *Biophys. J.* **2004**, *87*, 640−647.
(46) Fudge, D. S.; Gardner, K. H.; Forsyth, V. T.; Riekel, C.; Gosline, J. M. *Biophys. J.* **2003**, *85*, 2015−2027.
(47) Frisk, S.; Ikeda, R. M.; Chase, D. B.; Rabolt, J. F. *Appl. Spectrosc.* **2004**, *58*, 279−286.
(48) Lefèvre, T.; Rousseau, M.-E.; Pézolet, M. *Appl. Spectrosc.*, in press.
(49) Lagugné Labarthet, F.; Buffeteau, T.; Sourisseau, C. *Appl. Spectrosc.* **2000**, *54*, 699−705.
(50) Bower, D. I. *J. Polym. Sci., Part B: Polym. Phys.* **1981**, *19*, 93−107.
(51) Krimm, S.; Bandekar, J. *Adv. Protein Chem.* **1986**, *38*, 181−364.
(52) Rabolt, J. F.; Moore, W. H.; Krimm, S. *Macromolecules* **1977**, *10*, 1665−1074.

(53) Frushour, B. G.; Painter, P. C.; Koenig, J. L. *J. Macromol. Sci., Rev. Macromol. Chem.* **1976**, *C15*, 29−115.
(54) Edwards, H. G. M.; Farwell, D. W. *J. Raman Spectrosc.* **1995**, *26*, 901−909.
(55) Tsukada, M.; Freddi, G.; Monti, P.; Bertoluzza, A.; Kasai, N. *J. Polym. Sci., Part B: Polym. Phys.* **1995**, *33*, 1995−2001.
(56) Li, M. Z.; Tao, W.; Kuga, S.; Nishiyama, Y. *Polym. Adv. Technol.* **2003**, *14*, 694−698.
(57) Yukuhiro, K.; Kanda, T.; Tamura, T. *Insect Mol. Biol.* **1997**, *6*, 89−95.
(58) Sezutsu, H.; Yukuhiro, K. *J. Mol. Evol.* **2000**, *51*, 329−338.
(59) Scholtz, J. M.; Baldwin, R. L. *Annu. Rev. Biophys. Biomol. Struct.* **1992**, *21*, 95−118.
(60) Marqusee, S.; Robbins, V. H.; Baldwin, R. L. *Proc. Natl. Acad. Sci. U.S.A.* **1989**, *86*, 5286−5290.
(61) Spek, E. J.; Olson, C. A.; Shi, Z.; Kallenbach, N. R. *J. Am. Chem. Soc.* **1999**, *121*, 5571−5572.
(62) Ingwall, R. T.; Scheraga, H. A.; Lotan, N.; Berger, A.; Katchalski, E. *Biopolymers* **1968**, *6*, 331−368.
(63) Hronska, M.; van Beek, J. D.; Williamson, P.; Vollrath, F.; Meier, B. *Biomacromolecules* **2004**, *5*, 834−839.
(64) Vass, E.; Hollosi, M.; Besson, F.; Buchet, R. *Chem. Rev.* **2003**, *103*, 1917−1954.
(65) Bandekar, J.; Krimm, S. *Biopolymers* **1980**, *19*, 31−36.
(66) Krimm, S.; Bandekar, J. *Biopolymers* **1980**, *19*, 1−29.
(67) Hsu, S. L.; Moore, W. H.; Krimm, S. *Biopolymers* **1976**, *15*, 1513−1528.
(68) Tu, A. T. Proteins. *Raman Spectroscopy in Biology: Principles and Applications*; John Wiley & Sons: Chichester, U.K., 1982; Chapter 3, pp 65−116.
(69) Asakura, T.; Murakami, T. *Macromolecules* **1985**, *18*, 2614−2619.
(70) Asakura, T.; Nakazawa, Y. *Macromol. Biosci.* **2004**, *4*, 175−185.
(71) Kataoka, K.; Uematsu, I. *Kobunshi Ronbunshu* **1977**, *34*, 37−41.
(72) Rintoul, L.; Carter, E. A.; Stewart, S. D.; Fredericks, P. M. *Biopolymers* **2000**, *57*, 19−28.
(73) Yoshimizu, H.; Mimura, H.; Ando, I. *J. Mol. Struct.* **1991**, *246*, 367−379.
(74) Yoshimizu, H.; Mimura, H.; Ando, I. *Macromolecules* **1991**, *24*, 862−866.
(75) Cao, J. *J. Mol. Struct.* **2002**, *607*, 69−75.

BM060280W